DETECTING LANDSLIDE LOCATION USING KOMSAT 1AND IT'S USING LANDSLIDE-SUSCEPTIBILITY MAPPING

Saro Lee, Moungjin Lee

Geoscience Information Center, Korea Institute of Geoscience & Mineral Resources (KIGAM), 30, Gajung-dong, Yusung-gu, Daejeon, 305-350, Korea, E-mail : leesaro@kigam.re.kr
Environmental Information Center, Korea Environment Institute(KEI), 613-2 Bulgwang-dong, Eunpyeong-Gu, Seoul, 122-706, Korea, E-mail : leemj@kei.re.kr

ABSTRACT : The aim of this study was to detect landslide using satellite image and apply the landslide to probabilistic landslide-susceptibility mapping at Gangneung area, Korea using a Geographic Information System (GIS). Landslide locations were identified by change detection technique of KOMSAT-1 (Korea Multipurpose Satellite) EOC (Electro Optical Camera) images and checked in field. For landslide-susceptibility mapping, maps of the topography, geology, soil, forest, lineaments, and land cover were constructed from the spatial data sets. Then, the sixteen factors that influence landslide occurrence were extracted from the database. Using the factors and detected landslide, the relationships were calculated using frequency ratio, one of the probabilistic model. Then, landslide-susceptibility map was drawn using the frequency ration and finally, the map was verified by comparing with existing landslide locations. As the verification result, the prediction accuracy showed 86.76%. The landslide-susceptibility map can be used to reduce hazards associated with landslides and to land cover planning.

KEY WORDS: Landslide, Change Detection, GIS, Gangneung

1. INTRODUCTION

Landslides are major natural geological hazards and each year is responsible for enormous property damage and both direct and indirect costs. Korea experiences frequent landslides, with the most recent occurring in 1996, 1998, 1999, 2002 and 2006. They often result in significant damage to people and property. From 20 to 31 August, typhoon Rusa has hit Gangneung area by storm and heavy rainfall. The day-rainfall was 609mm and hour-rainfall was 80mm. As the result, 266 people died and the damage to property was about a value of 8 billion. Among this, the 81 people died by landslide and collapse of cut-slope. So, the Gangneung area was considered as study area. Especially, among the Gangneung area, the Sagimakri area is selected as study area because one of the most landslides occurred area. The study area lies between the 37° 45' N and 37° 50' N, and 128° 45' E and 128° 50' E, and covers an area of 47.94 km^2 (Fig. 1). The geology is the study area is Granite.

In Gangneung, much damage was caused by the landslides, which were due to the heavy rainfall, and, because there was little effort to assess or predict the event, damage was extensive. Through scientific analysis of landslides, we can assess and predict landslide-susceptible areas and, by allowing proper preparation, decrease landslide damage. In order to achieve this, the landslide locations were detected using satellite image and landslide-susceptibility analysis techniques were applied and verified using a frequency ratio model.

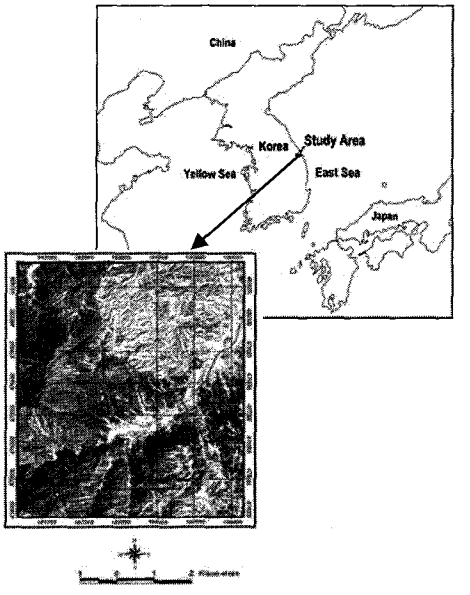

Figure 1. The study area with KOMSAT-1 EOC image.

2. LANDSLIDE-LOCATION DETECTION USING SATELLITE IMAGES

For probabilistic landslide hazard analysis, accurate detection of the location of landslides is very important. The application of remote sensing methods, such as aerial photographs and satellite imagery, is used to obtain significant and cost-effective information on landslides. A field survey of the study area is the most exact detection method. However, using field surveys as the initial method is difficult, time-consuming and costly, especially in mountainous areas where access is difficult or even impossible. Thus, limited data are collected, and it is

impossible to use complete landslide data in a probability analysis. A field survey can be used to verify the result of aerial photograph interpretation and satellite image analysis.

In this study, 6.6m-resolution KOMSAT-1 EOC images were used. This satellite takes images over a 24-day period in the same area, so that the satellite images can be compared before and after a landslide event. However, resolution of the image (6.6m) can't distinguish small-scale landslides. The KOMSAT-1 ECO images used to detect the landslide are December 7, 2001) (taken before the landslides occurred) and December 14, 2002) (after the landslides occurred). For change detection, image difference method was used.

For change detection, the images were preprocessed by doing geometric correction. The accurate geometrical correction is very imported for change detection. So, the image to image correction method has been applied. One image was corrected geometrically using 1:5,000 scale digital topographic map and the other image was corrected geometrically using the previous image. The second phase of preprocessing was done by atmospheric correction. For the atmospheric correction, the image-based model was used because the model doesn't need the information about atmospheric status of the image during time of acquisition. Then, the histogram of the image were matched by moving the histogram.

To make the change detection map, there are many methods available such as band ratio, principal components analysis and red green difference image. Among the methods, the red green difference method is used widely because the changed area can be seen directly in red green difference method when pixel value decreased, the pixel is viewed in Red color and when pixel value is increased, the pixel is viewed in greed color. This method is generally used wherever the change is distinct. The image acquired after landslide occurrence was used as red color layer. Then the landslide occurred area, only the green color was shown because of the increase in pixel value.

The landslide occurred areas are shown in Fig. 2. The change detection reveals many changes; for example, clouds, urban growth, river sediment change, and the landslide. The changes that are not related to landslides were excluded. Finally, based on the changed areas and damaged areas which was surveyed by Gangwon Province, the estimated landslide areas were selected. Then the selected area was checked by the field survey using GPS and 1:5,000 scale topographic maps. In total, 456 landslides were mapped within a total study area of 47.94 km^2. In this study area, the most of landslide is soil slide and debris flow.

Figure 2. Detected landslides.

3. DATA

Identification and mapping of a suitable set of instability factors bearing a relationship to slope failures requires an a priori knowledge of the main causes of landslides (Guzzetti *et al.*, 1999). These instability factors include surface and bedrock lithology and structure, bedding altitude, seismicity, slope steepness and morphology, stream evolution, groundwater conditions, climate, vegetation cover, land-use, and human activity. The availability of thematic data varies largely, depending on the type, scale, and method of data acquisition.

Table 1. Data layer of study area

Classification	Sub-Classification	Data Type	Scale
Geological Hazard	Landslide	Point coverage	1:5,000
Basic Map	Topographic Map	Line and Point coverage	1:5,000
	Geological Map		1:250,000
	Lineament Map	Polygon coverage	1:50,000
	Drainage Lineament Map		1:5,000
	Soil Map	Line coverage	1:25,000
	Forest Map	Line coverage	1:25,000
		Polygon coverage	
		Polygon coverage	
Image Data	Landsat TM	GRID	30m x 30m
	Land Use	GRID	5m x 5m
	KOMSAT Satellite Image	Image	6.6m x 6.6m

Sixteen factors were considered in calculating the probability. The factors were extracted from the constructed spatial database.

There were converted to ArcGIS GRID format and the GRID set comprised 1,586 rows by 1,209 columns, for a total cell number of 1,917,474. Landslides had occurred in 456 of these cells.

4. METHODOLOGY

The spatial relationships between the landslide location and each landslide-related factor were analysed by using the probability model - frequency ratio. The frequency ratio, a ratio between the occurrence and absence of landslides in each cell, was calculated for each factor's type or range that had been identified as significant with respect to causing landslides. The ratios of each factor's type or range were summed to calculate the landslide susceptibility index (LSI), as shown in Eq. (1):

$$LSI = \Sigma Fr \quad (1)$$

where Fr = the frequency ratio of each factors' type or range.

Using the LSI, landslide susceptibility map was made. Finally, the susceptibility map was verified using existing landslide locations. In this study, these two assumptions are satisfied because the landslides are related to the spatial information and all the landslides were precipitated by a single cause, namely, heavy rainfall in the Gangneung areas. For the verification, the calculated LSI values of all cells in the study area were sorted in descending order for all nine cases. Then, the landslides (%) were divided into classes of accumulated area ratio (%) according to the LSI value. To compare the result quantitative, the areas under the curve (AUC) were re-calculated as the total area is 1 which means perfect prediction accuracy. So, the AUC can be used to assess the prediction accuracy qualitatively.

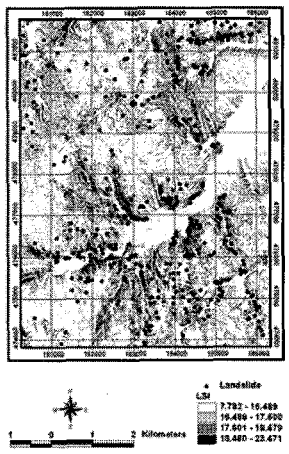

Figure 3. Landslides susceptibility maps using frequency ratio model

5. LANDSLIDE SUSCEPTIBILITY MAPPING AND VERIFICATION

Using the frequency ratio and Eq. (1), the LSI values were computed. The computed LSI values were mapped to allow interpretation such as that illustrated in Fig. 3. The LSI values were classified into four classes (highest 10%, second 10%, third 20% and reminding 60%) based on area for visual and easy interpretation.. If the LSI value is high, there is a higher susceptibility to landslides; a lower value indicates a lower susceptibility to landslides. The minimum, mean, maximum and standard deviation values of LSI are 7.78 16.00, 23.47 and 2.00 respectively.

The results of the landslide susceptibility analysis were verified using the landslide locations for the same study areas. The 90–100% (10%) class with the highest probability of a landslide contains 54% of the landslides (Fig. 4). The 80–100% class (20%) contains 75% and the 70-100% class (30%) contains 88% of the landslides of Sagimakri area. To compare the result quantitative, the AUC were re-calculated as the total area is 1. The area ratio was 0.8676 and I could say the prediction accuracy is 86.76%.

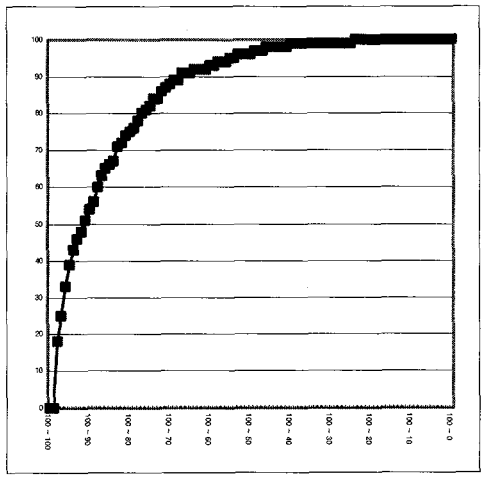

Figure 4. . Illustration of cumulative frequency diagram showing landslide susceptibility index rank (x-axis) occurring in cumulative percent of landslide occurrence (y-axis)

6. DISCUSSION AND CONCLUSIONS

Landslides are among the most hazardous of natural disasters. Government and research institutions worldwide have attempted for years to assess landslide hazard and risk and to predict their spatial distribution. In this study, detection of landslide using satellite image and application of a probabilistic approach to estimating the susceptible areas is presented using image process and GIS. As the result, prediction accuracy showed the 86.76%. Generally, the verification results showed satisfactory agreement between the susceptibility map and the existing data on landslide location.

In this study, only the susceptibility analysis was performed because the small area studied did not allow us

to determine the distribution of rainfall. However, if data on factors causing the landslides (such as rainfall, earthquakes or slope cutting) exist, then a possibility analysis could also be done. In particular, if the data could be combined with a hydrological model, a more accurate analysis would be possible. If the factors relevant to the vulnerability of buildings and other property were available, a risk analysis could also be done. Landslide susceptibility maps are of great help to planners and engineers choosing suitable locations for development. These results can be used as basic data to assist slope management and land-use planning.

Table 2. Spatial relationship between landslide and related factors in Sagimakri area

Factor	Class	No of pixels in domain	% of domain	No of landslide	% of landslide	Ratio
Slope	0 ~ 5	336945	17.57	0	0.00	0.00
	6 ~ 10	204758	10.68	2	0.44	0.04
	11 ~ 15	311658	16.25	13	2.85	0.18
	16 ~ 20	362062	18.88	48	10.53	0.56
	21 ~ 25	322133	16.80	93	20.39	1.21
	26 ~ 30	217740	11.36	157	34.43	3.03
	31 ~ 35	108568	5.66	99	21.71	3.83
	36 ~ 40	39827	2.08	29	6.36	3.06
	41 ~ 90	13783	0.72	15	3.29	4.58
Aspect	Flat	82385	4.30	0	0.00	0.00
	North	226606	11.82	31	6.80	0.58
	Northeast	292155	15.24	56	12.28	0.81
	East	299541	15.62	77	16.89	1.08
	Southeast	247143	12.89	49	10.75	0.83
	South	165431	8.63	62	13.60	1.58
	Southwest	169659	8.85	46	10.09	1.14
	West	209333	10.92	78	17.11	1.57
	Northwest	225221	11.75	57	12.50	1.06
Curvature	Concave	557948	29.10	136	29.82	1.02
	Flat	785003	40.94	129	28.29	0.69
	Convex	574523	29.96	191	41.89	1.40
Distance from Water	Buffer(100m)	1421849	74.15	330	72.37	0.98
	Buffer(200m)	374666	19.54	102	22.37	1.14
	Buffer(300m)	86849	4.53	17	3.73	0.82
	Buffer(400m)	29718	1.55	7	1.54	0.99
	Buffer(> 400m))	4392	0.23	0	0.00	0.00
Geology	Granite	1894865	98.82	456	100.00	1.01
	Alluvial deposit	22609	1.18	0	0.00	0.00
Distance from Lineament	Buffer(100m)	466283	24.32	235	51.54	2.12
	Buffer(200m)	425867	22.21	116	25.44	1.15
	Buffer(300m)	325061	16.95	44	9.65	0.57
	Buffer(400m)	242507	12.65	27	5.92	0.47
	Buffer(500m)	178295	9.30	20	4.39	0.47
	Buffer(> 500m))	279461	14.57	14	3.07	0.21
Soil Texture	Sandy loam	915636	47.75	47.75	61.18	1.28
	Fine sandy loam	8648	0.45	0.45	0.00	0.00
	Gravelly sandy loam	2625	0.14	0.14	0.22	1.60
	Loam	35391	1.85	1.85	0.88	0.48
	Silt loam	32060	1.67	1.67	0.00	0.00
	Gravelly loam	27715	1.45	1.45	1.10	0.76
	Overflow area	43180	2.25	2.25	0.44	0.19
	Rocky sandy	627654	32.73	32.73	30.92	0.94
	Rocky loam	224294	11.70	11.70	5.26	0.45
	Gravelly sandy	271	0.01	0.01	0.00	0.00
Soil Drainage	No data	43180	2.25	2	0.44	0.19
	Poorly drained	110409	5.76	9	1.97	0.34
	Somewhat poorly drained	97606	5.09	26	5.70	1.12
	Moderately well drained	25422	1.33	4	0.88	0.66
	Well drained	191337	9.98	32	7.02	0.70
	Excessively drained	1449520	75.60	383	83.99	1.11
Soil Material	No data	43180	2.25	2	0.44	0.19
	Colluvium	42908	2.24	6	1.32	0.59
	Valley alluvium	289190	15.08	62	13.60	0.90
	Granite residuum	1256190	65.51	362	79.39	1.21
	Fluvial alluuium	61712	3.22	0	0.00	0.00
	Pluton residuum	224294	11.70	24	5.26	0.45
Soil Thickness	No data	43180	2.25	2	0.44	0.19
	Poorly shallow	7484	0.39	0	0.00	0.00
	Shallow	846156	44.13	165	36.18	0.82
	Normal	984026	51.32	284	62.28	1.21
	Deep	36628	1.91	5	1.10	0.57
Forest Type	Non-forest	22.55	117	25.66	1.14	1.14
	Borad leaf tree	1.87	9	1.97	1.06	1.06
	Pine	54.06	253	55.48	1.03	1.03
	Cultivated	3.18	13	2.85	0.90	0.90
	Paper pulp	0.03	0	0.00	0.00	0.00
	Artificial pine	0.70	7	1.54	2.18	2.18
	Larch	4.38	18	3.95	0.90	0.90
	Korea nut pine	8.04	21	4.61	0.57	0.57
	Artificial rigida pine	0.29	3	0.66	2.31	2.31
	Mixing tree	4.90	15	3.29	0.67	0.67
Forest Diameter	Non-forest	493960	25.76	130	28.51	1.11
	Very small diameter (below 6cm)	262481	13.69	54	11.84	0.87
	Small diameter (6 ~ 16cm)	884637	46.14	230	50.44	1.09
	Medium diameter (16 ~ 28cm)	276396	14.41	42	9.21	0.64
Forest Age	Non-forest	493960	25.76	130	28.51	1.11
	More than 50% 1 ~ 10 years old timber	262481	13.69	54	11.84	0.87
	More than 50% 11 ~ 20 years old	595802	31.07	184	40.35	1.30
	More than 50% 21 ~ 30 years old timber	301220	15.71	47	10.31	0.66
	More than 50% 31 ~ 40 years old timber	242658	12.66	35	7.68	0.61
	More than 50% 41 ~ 50 years old timber	21353	1.11	6	1.32	1.18
Forest Density	Non-forest	756441	39.45	184	40.35	1.02
	Loose	873578	45.56	196	42.98	0.94
	Moderate	200765	10.47	54	11.84	1.13
	Dense	86690	4.52	22	4.82	1.07
Land Cover	No data	0	0.00	0	0.00	0.00
	Water	4824	0.25	1	0.22	0.87
	Urban	40134	2.09	20	4.39	2.10
	Forest	1715778	89.49	400	87.72	0.95
	Grass	45504	2.37	6	1.32	0.55
	Rice field	106446	5.55	27	5.92	1.07
	Barren	4680	0.24	2	0.44	1.80

References

Atkinson, P.M., Massari, R. Generalized linear modeling of susceptibility to landsliding in the central Apennines, Italy. Computer & Geosciences 24 (4), 373-385, 1998.

Baeza, C., Corominas, J. Assessment of shallow landslide susceptibility by means of multivariate statistical techniques earth surface processes and landforms 26, 1251-1263, 2001.

Lee, S ., Choi, J., Min, K. Landslide susceptibility analysis and verfication using the Bayesian probability model, Environmental Geology. 43, 120-131, 2002a.

Lee, S., Chwae, U., Min, K. Landslide susceptibility mapping by correlation between topography and geological structure: the Janghung area, Korea. Geomorphology 46, 149-162, 2002b.

Lee, S., Ryu, J.H., Min, K., Won, J.S. Landslide Susceptibility Analysis using GIS and Artificial neural network. Earth Surface Processes and Landforms 27, 1361-1376, 2003a.

Lee, S., Ryu, J.H., Lee, M.J., Won, J.S. Landslide susceptibility analysis using artificial neural network at Boeun, Korea. Environmental Geology 44, 820-833, 2003b,

Lee, S., Choi, U. Development of GIS-based geological hazard information system and its application for landslide analysis in Korea. Geoscience Journal 7, 243-252, 2003c.

Lee, S., Ryu, J.H., Won, J.S., Park, H.J. Determination and application of the weights for landslide susceptibility mapping using an artificial neural network. Engineering Geology 71, 289-302, 2004a.

Lee, S., Choi, J., Min, K. Probabilistic Landslide Hazard Mapping using GIS and Remote Sensing Data at Boeun, Korea. International Journal of Remote Sensing 25, 2037-2052, 2004b.